Regular Article

Catalytic oxidation of dibromomethane over Ti-modified Co_3O_4 catalysts: Structure, activity and mechanism

Jian Mei, Wenjun Huang, Zan Qu, Xiaofang Hu, Naiqiang Yan *

School of Environmental Science and Engineering, Shanghai Jiao Tong University, 800 Dong Chuan Road, Shanghai 200240, PR China

GRAPHICAL ABSTRACT
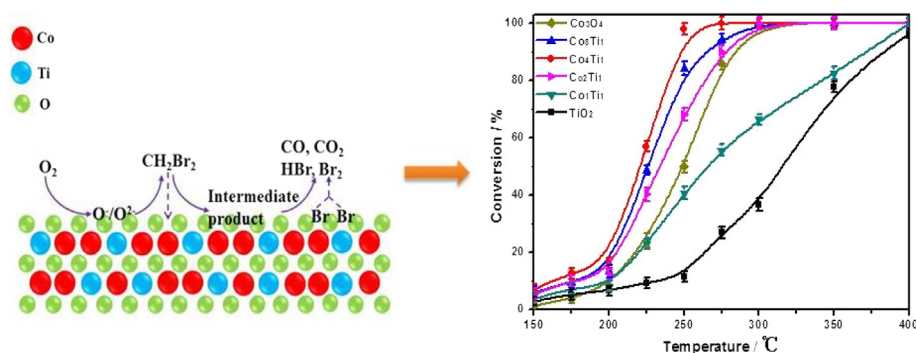
ARTICLE INFO

ABSTRACT

Ti-modified Co_3O_4 catalysts with various Co/Ti ratios were synthesized using the co-precipitation method and were used in catalytic oxidation of dibromomethane (CH_2Br_2), which was selected as the model molecule for brominated volatile organic compounds (BVOCs). Addition of Ti distorted the crystal structure and led to the formation of a Co-O-Ti solid solution. Co_4Ti_1 (Co/Ti molar ratio was 4) achieved higher catalytic activity with a T_{90} (the temperature needed for 90% conversion) of approximately 245 °C for CH_2Br_2 oxidation and higher selectivity to CO_2 at a low temperature than the other investigated catalysts. In addition, Co_4Ti_1 was stable for at least 30 h at 500 ppm CH_2Br_2, 0 or 2 vol% H_2O, 0 or 500 ppm p-xylene (PX), and 10% O_2 at a gas hourly space velocity of 60,000 h^{-1}. The final products were CO_x, Br_2, and HBr, without the formation of other Br-containing organic byproducts. The high catalytic activity was attributed to the high Co^{3+}/Co^{2+} ratio and high surface acidity. Additionally, the synergistic effect of Co and Ti made it superior for CH_2Br_2 oxidation. Furthermore, based on the analysis of products and *in situ* DRIFTs studies, a receivable reaction mechanism for CH_2Br_2 oxidation over Ti-modified Co_3O_4 catalysts was proposed.

© 2017 Elsevier Inc. All rights reserved.

1. Introduction

Of late years, with the frequent occurrence of serious haze pollution in China, there is growing concern over the abatement of volatile organic compounds (VOCs) as one of the vital precursors to the formation of secondary organic aerosol [1–3]. In addition to the atmosphere environment damage, many VOCs, like brominated volatile organic compounds (BVOCs), are cancerigenic and pernicious to human health and safety [4]. BVOCs are emitted by several aspects, including pesticide and petrochemical industry. Additionally, BVOCs are typically released from purified terephthalic acid

---

* Corresponding author.
  E-mail address: nqyan@sjtu.edu.cn (N. Yan).

(PTA) exhaust gas, and their treatment is both an urgent task and a challenge because of their refractory to degradation [5]. Among all the technologies we have for BVOCs abatement, catalytic oxidation is an economical-efficient technology for oxidation of BVOCs to CO_2, H_2O, and other less detrimental compounds and is regarded as the most promising technology for BVOCs abatement due to its low energy consumption and high efficiency [6].

In recent years, two types of catalysts, noble metals [7] and transition metal oxides [8], have been widely used in the catalytic oxidation of BVOCs. Generally, noble metal catalysts have high catalytic activity, but they have the disadvantages of a high cost and easy deactivation with bromine-poisoning. Increasing attention is being paid to transition metal oxides because of their acceptable catalytic activity and high resistance to bromine-poisoning, and developing transition oxidation catalysts with high catalytic activity and resistance to bromine-poisoning is promising.

Co_3O_4, which has a typical spinal structure, has been widely applied in the catalytic field. The high oxygen mobility and good redox properties of Co_3O_4 contribute to its excellent catalytic performance in total catalytic oxidation reactions [9]. According to our previous studies, its high catalytic activity for BVOCs oxidation over Co_3O_4-based catalysts is attributed to the unique redox properties [8,10]. Nevertheless, there is significantly improving space for BVOCs oxidation over Co_3O_4-based catalysts in terms of their catalytic activity, stability and product-selectivity. It has been reported that appropriate modification of Co_3O_4-based catalysts with other transition metal oxides can further promote catalytic activity and stability. For example, Cai et al. prepared Mn-modified Co_3O_4 catalysts with various Co/Mn ratios by co-precipitation method for 1,2-dichlorobenzene oxidation, and found that Co_9Mn_1 presented the highest activity and high stability at least for 35 h [11]. Additionally, the use of TiO_2 as a support has

been broadly researched in the field of catalytic oxidation of VOCs because of its high specific surface area and strong surface acidity [12–15]. However, no study on the behaviors of Ti-modified Co_3O_4 catalysts in the catalytic oxidation of BVOCs is reported.

In this study, a series of Ti-modified Co_3O_4 catalysts with various Co/Ti ratios was synthesized using the co-precipitation method, and the catalysts were used in catalytic oxidation of CH_2Br_2, which was selected as the model molecule for BVOCs. The physicochemical properties of Ti-modified Co_3O_4 catalysts were investigated, and the catalytic activity, product selectivity, and stability were also studied. Furthermore, based on the analysis of products and in situ DRIFTs studies, a receivable reaction mechanism for CH_2Br_2 oxidation over Ti-modified Co_3O_4 catalysts was proposed.

2. Experimental section

2.1. Materials

$Co(NO_3)_2 \cdot 6H_2O$ and ethanol were purchased from Pharmaceutical group co., Ltd. $Ti[O(CH_2)_3CH_3]_4$ was obtained from Shanghai Aladdin biochemical technology co., Ltd. Ammonia water was supplied by Shanghai ling feng chemical reagent co., Ltd. Ultrapure water with a resistivity of 18.2 MΩ cm produced from an ultrapure water purification system (Ulupure) were used to prepare all the solutions.

2.2. Catalyst preparation

A series of Ti-modified Co_3O_4 catalysts with various Co/Ti ratios was synthesized using the co-precipitation method. In a typical
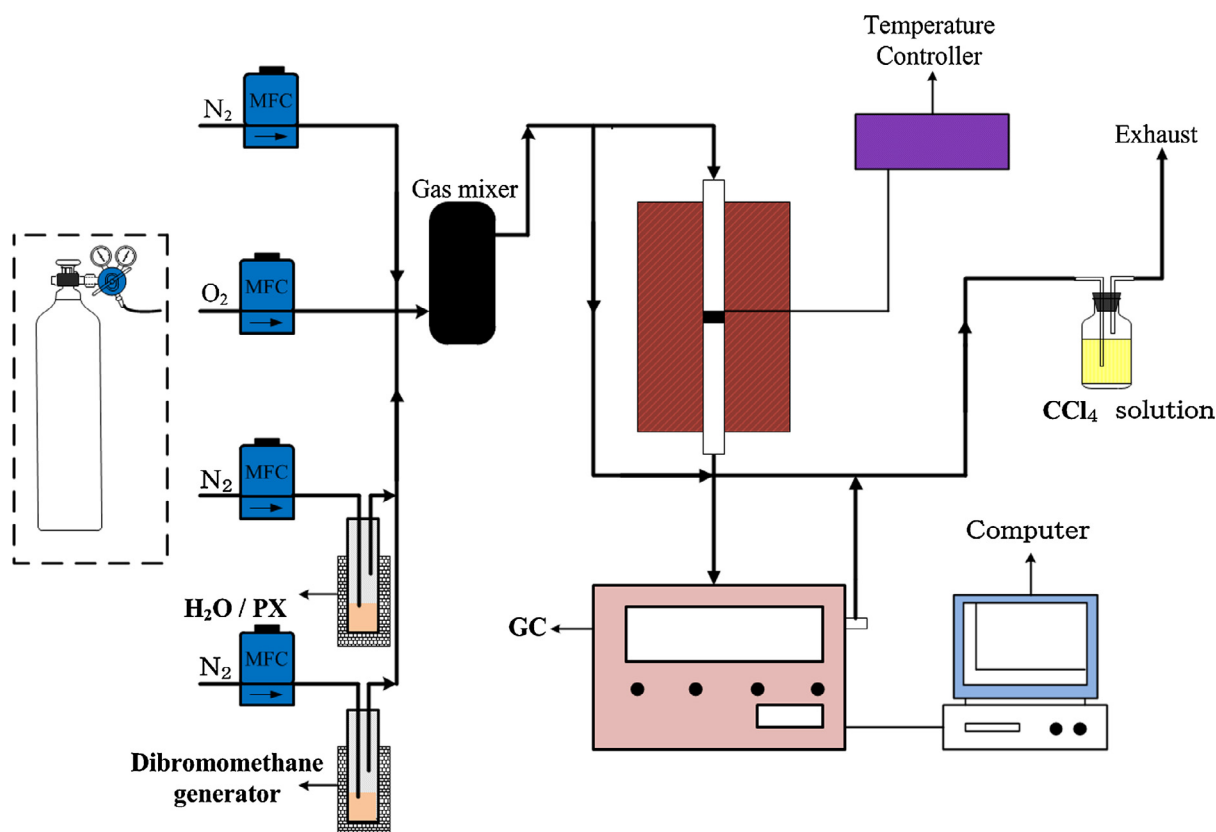
Fig. 1. A flow process of CH_2Br_2 catalytic system.
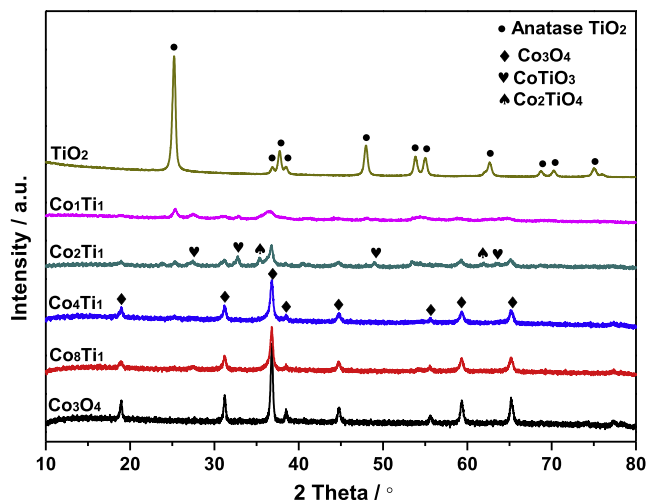
Fig. 2. XRD patterns of Ti-modified Co_3O_4 catalysts with various Co/Ti ratios.

synthesis process, $Co(NO_3)_2 \cdot 6H_2O$ was dissolved in 80 ml of ultra-pure water and $Ti[O(CH_2)_3CH_3]_4$ was dissolved in 20 ml of ethanol. Then, the two solutions were mixed together with various Co/Ti ratios and stirred for 3 h. Afterwards, 10 ml of ammonia water was added dropwise into the mixed solution and stirred for 2 h. Finally, the obtained precipitates were washed with ultrapure water three times and separated using suction filtration; then, they were dried at 90 °C for 10 h and calcined at 500 °C for 3 h. Pure Co_3O_4 and TiO_2 were prepared using the same method. The obtained samples with various Co/Ti ratios were marked Co_xTi_y, where x and y were based on the molar numbers of Co and Ti.

2.3. Catalyst characterization

Power X-ray diffraction patterns (XRD) were conducted on a Shimadzu XRD-6100, and the diffractograms were collected in the 2θ range of 10–80° with a scanning velocity of 10 °/min. The nitrogen adsorption-desorption isotherms were obtained using a physical adsorption instrument (Nova 2200e) at −196 °C. Prior to each experiment, the samples were pretreated in a vacuum at
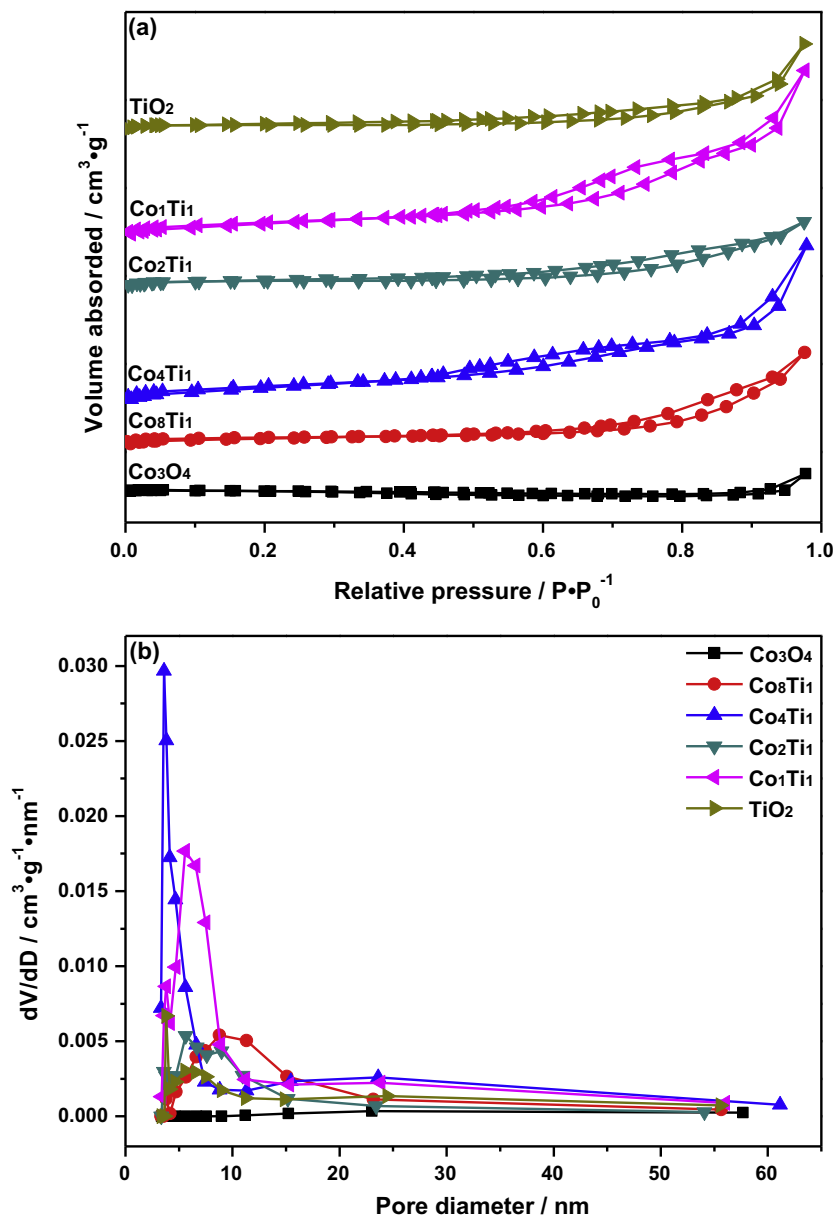
Fig. 3. N_2 adsorption-desorption isotherm (a) and pore size distribution (b) of Ti-modified Co_3O_4 catalysts.

Table 1
Physical properties of Ti-modified Co_3O_4 catalysts.

Catalyst	S_{BET} ($m^2\,g^{-1}$)	Average pore diameter (nm)	Average pore volume ($cm^3\,g^{-1}$)
Co_3O_4	0.2	23.02	0.02
Co_8Ti_1	18.9	8.79	0.09
Co_4Ti_1	46.3	3.59	0.15
Co_2Ti_1	15.9	5.64	0.06
Co_1Ti_1	40.4	5.56	0.16
TiO_2	19.3	3.80	0.08

200 °C for 3 h. The specific surface area was determined using a multi-point BET model, and pore size and pore volume were determined using a BJH model. Raman spectra were conducted on a SENTERRA R200 microscope. The microscopic morphology of the samples was observed using transmission electron microscopy (TEM) (JEOL-2100F). Before each experiment, the samples were evenly dispersed in ethanol solution under the condition of ultrasound. The excitation source was the 532 nm line of an Ar ion laser. The X-ray photoelectron spectroscopy (XPS) was conducted on a PHI-5300 (PE) spectrometer using Mg Ka radiation as an excitation source, and the binding energy was calibrated using the C 1s line at 284.8 eV as an internal standard. The H_2-temperature-programmed reduction (H_2-TPR) experiments were conducted on a chemical adsorption instrument (AutoChem II, 2920). Prior to each experiment, 50 mg samples were pretreated in Ar flow at 300 °C for 2 h. Next, after cooling to 100 °C, the samples were heated to 1000 °C in 10% H_2/Ar flow at a heating rate of 10 °C/min. The NH_3-temperature-programmed desorption (NH_3-TPD) experiments were also conducted on a chemical adsorption instrument (AutoChem II, 2920). Prior to each experiment, the 300 mg samples were pretreated in He flow at 300 °C for 2 h. Next, after cooling to 50 °C, NH_3 adsorption was performed in 10% NH_3/He flow at 50 °C for 1 h. Subsequently, the samples were treated in He flow for 30 min to remove physically adsorbed NH_3; then, they were heated to 800 °C in He flow at a heating rate of 10 °C/min. Thermogravimetric analysis (TGA) was performed using a Mettler Toledo analyzer, the pyrolysis process was performed from room temperature to 1000 °C at the heating rate of 10 °C/min, and Ar was fed at 50 mL/min as an inert purge gas.

2.4. Catalytic activity evaluation

The catalytic activity for CH_2Br_2 oxidation was evaluated using a fixed-bed flow reactor with an inner diameter of 6 mm, and a schematic representation of the CH_2Br_2 catalytic system is presented in Fig. 1. 90 mg of catalyst was sandwiched between two silica wool layers in the middle of the reactor. The gas feed is a mixture of 500 ppm CH_2Br_2, 10% O_2, 0 or 500 ppm p-xylene (PX), 0 or 2 vol% H_2O, and N_2 as the balance. The gaseous CH_2Br_2 was produced by the nitrogen-blowing method, passing N_2 flow through a bottle containing pure CH_2Br_2 liquid in a homoisothermal oil bath, and the gaseous PX and H_2O were produced by the same method. The total gas flow was 150 ml/min, resulting in a gas hourly space velocity (GHSV) of 60,000 h^{-1}. The reaction temperature was controlled by an electrical furnace. The concentrations of CH_2Br_2 in the inlet and outlet were determined using a GC-2010 Plus system fitted with an FID and were collected at each evaluated temperature after 30 min of the stability. The catalytic activity was evaluated in accordance with CH_2Br_2 conversion, which was defined as follows:

$$X_{CH_2Br_2} = \frac{C_{in} - C_{out}}{C_{in}} \times 100\% \tag{1}$$

where C_{in} and C_{out} are the CH_2Br_2 concentrations that correspond to the inlet and outlet, respectively.

The outlet gas products were determined using a GCMS-QP2010 system. The concentrations of HBr and Br_2 were monitored using the titration method. First, the gas flow containing HBr and Br_2 was fully absorbed in a KI solution. Second, the concentration of Br_2 was monitored by titration using $Na_2S_2O_3$ solution with starch solution as an indicator. The concentration of bromide ions in the absorbed solution was monitored by an ion chromatography. The concentrations of CO and CO_2 were determined using a GC-14B system fitted with an FID and methane conversion oven. The selectivity to CO, CO_2, HBr, and Br_2 were, respectively, defined as follows:

$$s_{co} \frac{C_{co}}{C_{in} - C_{out}} \times 100\% \tag{2}$$
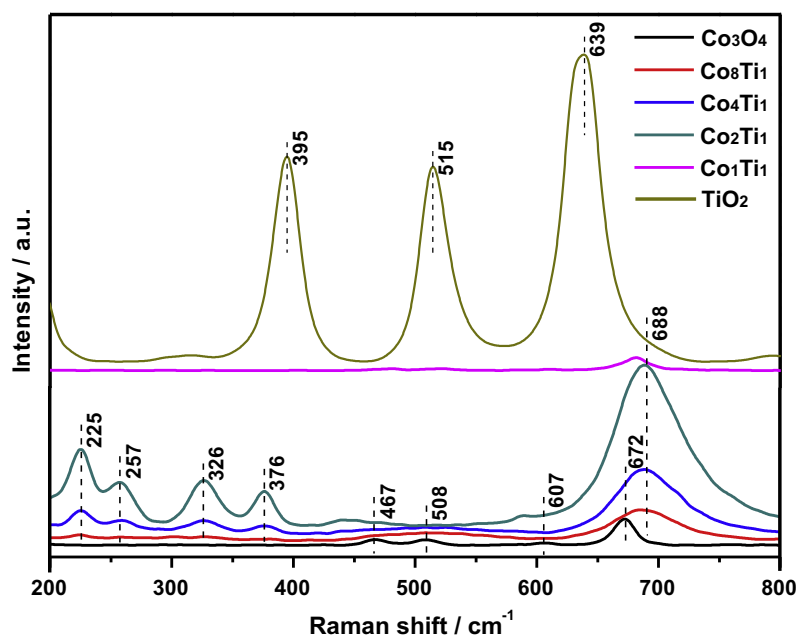
Fig. 4. Raman spectra of Ti-modified Co_3O_4 catalysts with various Co/Ti ratios.
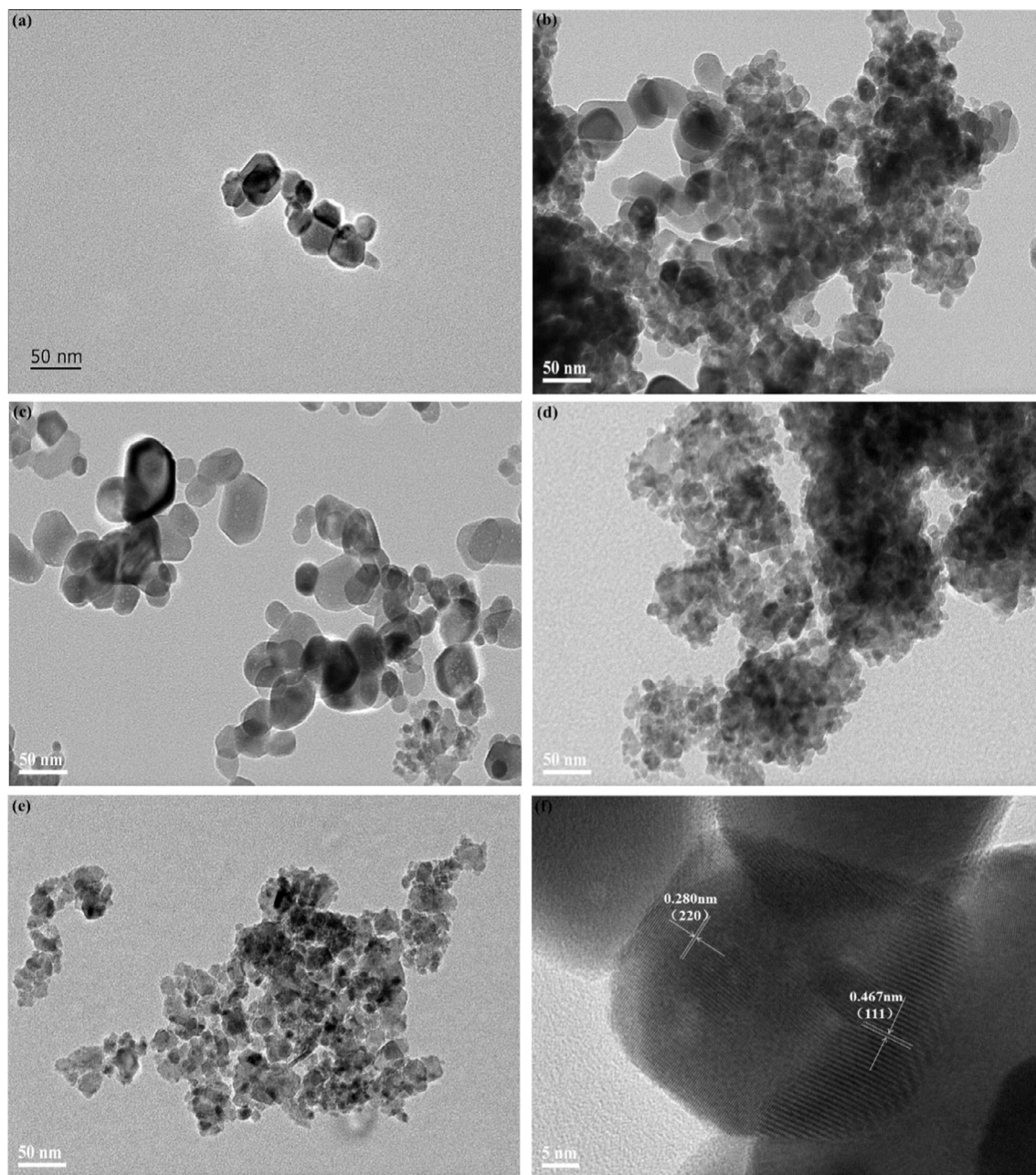
Fig. 5. TEM images of Co_3O_4 (a), Co_8Ti_1 (b), Co_4Ti_1 (c), Co_2Ti_1 (d), Co_1Ti_1 (e) and HRTEM image of Co_4Ti_1 (f).

$$S_{CO_2} = \frac{C_{co_2}}{C_{in} - C_{out}} \times 100\% \qquad (3)$$

$$S_{HBr} = \frac{C_{HBr}}{2(C_{in} - C_{out})} \times 100\% \qquad (4)$$

$$S_{Br_2} = \frac{C_{Br_2}}{C_{in} - C_{out}} \times 100\% \qquad (5)$$

where C_{co} and C_{co2} are the concentrations of CO and CO_2 (ppm) in the outlet, and C_{HBr} and C_{Br_2} are the concentrations of Br_2 and HBr (ppm) in the outlet.

2.5. In situ DRIFTs study

In situ DRIFTs experiments were conducted on a Fourier transform infrared spectrometer (FTIR, Nicolet 6700) fitted with an MCT detector. The DRIFTs cell was fitted with ZnSe windows and a heating chamber. The reaction conditions were simulated using a temperature controller and mass flow controllers. Spectra were collected in the range of 4000 to 800 cm^{-1} at a resolution of 4 cm^{-1} and over 100 scans. Prior to each experiment, the samples were pretreated with 10% O_2/N_2 at 400 °C for 2 h to purify the catalyst surface and they were then cooled to 50 °C. Spectra of the clean catalyst surface was collected at each evaluated temperature and used as the background. Next, a gas flow containing 500 ppm of CH_2Br_2/10% O_2/N_2 was exposed to the DRIFTs cell at 50 °C for 1 h. Finally, the catalyst was treated in 10% O_2/N_2 from 50 to 350 °C, and the spectra were collected from 50 to 350 °C.
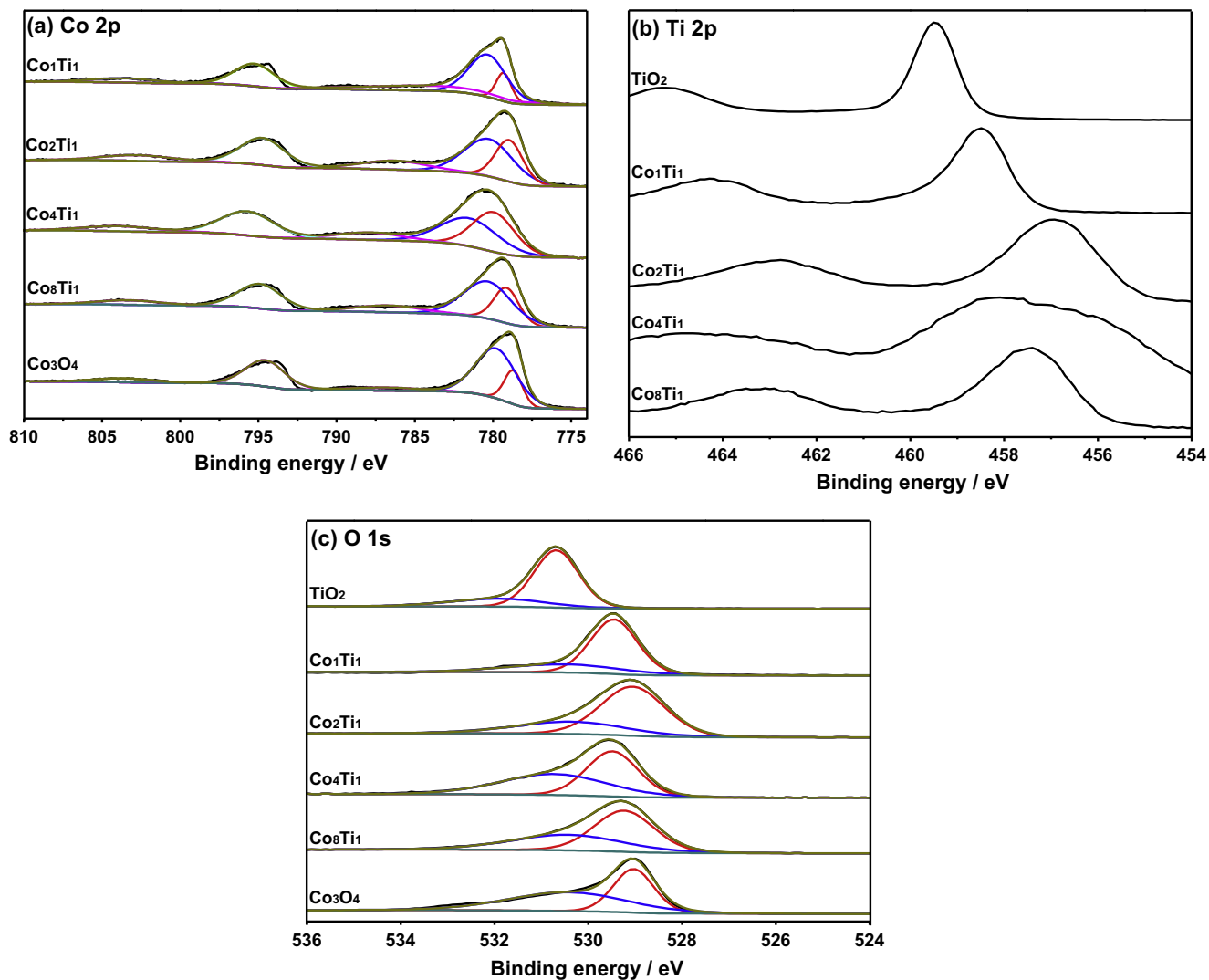
Fig. 6. XPS spectra of Ti-modified Co_3O_4 catalysts with various Co/Ti ratios: (a) Co $2p_{3/2}$, (b) Ti 2p and (c) O 1s.

Table 2
XPS analysis of the fresh Ti-modified Co_3O_4 catalysts.

Catalyst	Co^{3+}/Co^{2+}	O_{ads}/O_{lat}
Co_3O_4	0.30	1.27
Co_8Ti_1	0.50	0.71
Co_4Ti_1	1.02	0.96
Co_2Ti_1	0.62	0.43
Co_1Ti_1	0.27	0.35
TiO_2	–	0.29

3. Results and discussion

3.1. Catalyst characterization

The XRD patterns of Ti-modified Co_3O_4 catalysts are presented in Fig. 2. For Ti-modified Co_3O_4 catalysts with a Co/Ti ratio of 2 or higher, eight diffraction peaks were observed at 2θ values of 19.0, 31.3, 36.9, 38.6, 44.9, 55.7, 59.4, and 65.3°, which were consistent with the Co_3O_4 spinal phase (JPCDS: 43-1003) [16], and the diffraction peaks ascribed to TiO_2 were not detected. However, the diffraction peaks of Co_3O_4 spinel became weaker and broader with increasing Ti content, which suggested a decrease in the size

of the Co_3O_4 spinel particle. Additionally, for Co_2Ti_1, several weak peaks at 27.4, 32.7, 48.9, and 63.6° were ascribed to $CoTiO_3$ (JCPDS: 77-1373) [17], and those at 35.4 and 62.0° were assigned to Co_2-TiO_4 (JCPDS: 39-1410) [18], indicating that Co-O-Ti solid solutions were formed. Because the radius of Ti^{4+} (0.0605 nm) was smaller than that of Co^{3+} (0.061 nm), it was possible that Ti^{4+} was incorporated into the Co_3O_4 spinel lattice. However, the diffraction peaks ascribed to $CoTiO_3$ and Co_2TiO_4 were not observed for Ti-modified Co_3O_4 catalysts with a Co/Ti ratio of 4 or higher, indicating that $CoTiO_3$ and Co_2TiO_4 had transitioned into the spinel phase. Interestingly, Co_1Ti_1 only exhibited weak peaks at 25.3 and 36.9 , and no other obvious diffraction peaks of Co_3O_4 spinel or TiO_2 were observed, indicating that the Co_1Ti_1 crystallinity was inferior and the particle sizes were also very small. For pure TiO_2, diffraction peaks at 25.3, 36.8, 37.7, 38.5, 48.0, 53.8, 62.6, 68.8, 70.3, and 75.0° were observed, indicating TiO_2 existed in the anatase form (JCPDS: 40-1290) [19].

The N_2 adsorption-desorption isotherm and pore size distribution of Ti-modified Co_3O_4 catalysts are presented in Fig. 3, and the physical properties estimated using the N_2 physisorption are listed in Table 1. As shown in Fig. 3(b), the pore size distribution of pure Co_3O_4 was in the range of 10–60 nm, which was calculated using the N_2 adsorption-desorption isotherm based on the BJH
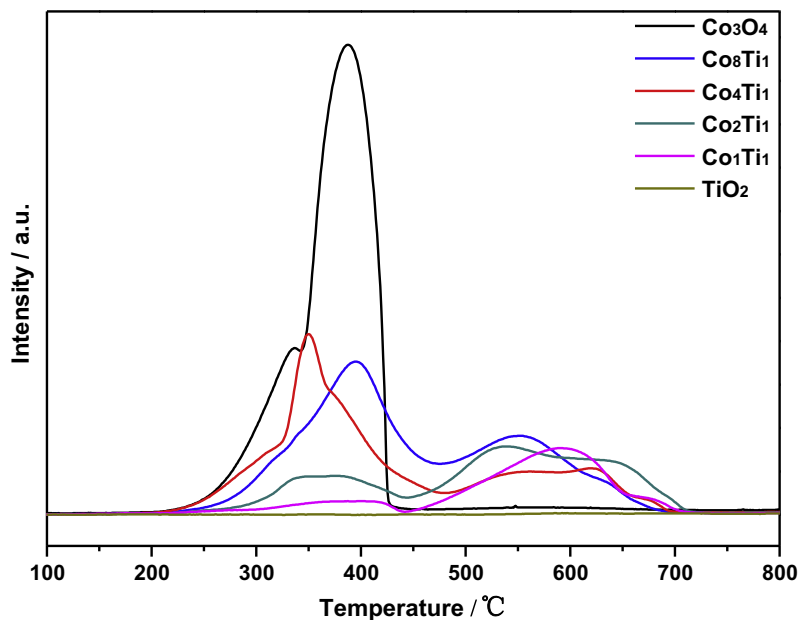
Fig. 7. H$_2$-TPR profiles of Ti-modified Co$_3$O$_4$ catalysts with various Co/Ti ratios.
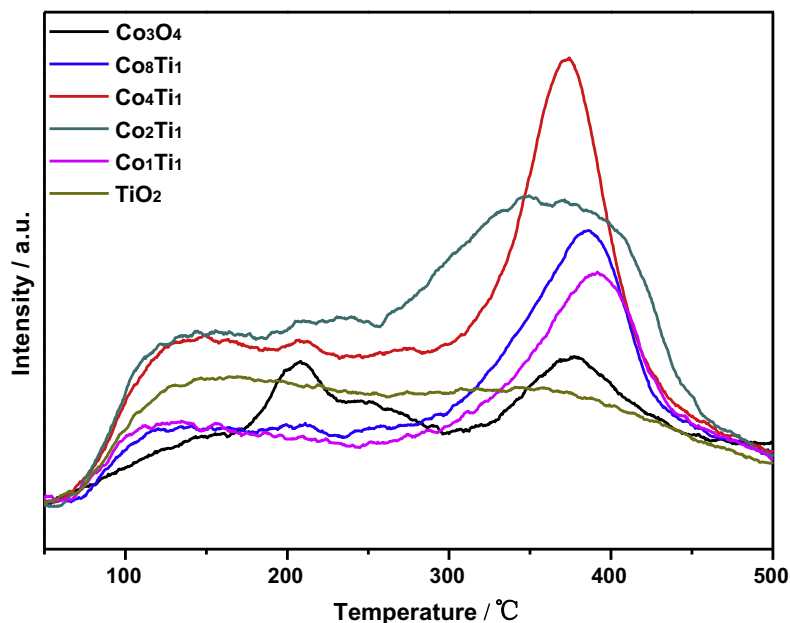
Fig. 8. NH$_3$-TPD profiles of Ti-modified Co$_3$O$_4$ catalysts with various Co/Ti ratios.

model. With the incorporation of Ti species, the pore size became small. Co$_4$Ti$_1$ had the smallest average pore diameter, and its pore size was concentrated on 3 nm. Moreover, compared with pure Co$_3$O$_4$ (0.2 m^2 g^{-1}), the BET specific surface areas of Ti-modified Co$_3$O$_4$ catalysts significantly increased, indicating that the dispersion of Ti-modified Co$_3$O$_4$ catalysts increased. Additionally, Co$_4$Ti$_1$ had the largest BET specific surface area (46.3 m^2 g^{-1}), which favored improving the catalytic activity. However, pure TiO$_2$ only had a small BET specific surface area (19.3 m^2 g^{-1}).

To further understand the phase structure of Ti-modified Co$_3$O$_4$ catalysts, Raman was conducted to precisely define the lattice structure of the Ti-modified Co$_3$O$_4$ catalysts in combination with XRD, and the results are presented in Fig. 4. In the range of 200–800 cm^{-1}, pure Co$_3$O$_4$ showed four typical bands that corresponded to the vibration modes of Co$_3$O$_4$ spinel (E$_g$ mode at 467 cm^{-1}, F$_{2g}$ mode at 607 and 508 cm^{-1}, and A$_{1g}$ mode at 672 cm^{-1}) [20]. With the incorporation of Ti, Raman bands that were attributed to the Co$_3$O$_4$ spinel structure became broader and weak. Meanwhile, some new bands at 225, 257, 326, 376, and 688 cm^{-1} were observed, and they became stronger with increasing Ti content. The former four bands corresponded to Co$_2$-TiO$_4$ [21], and the latter one was related to CoTiO$_3$ [22]. The results
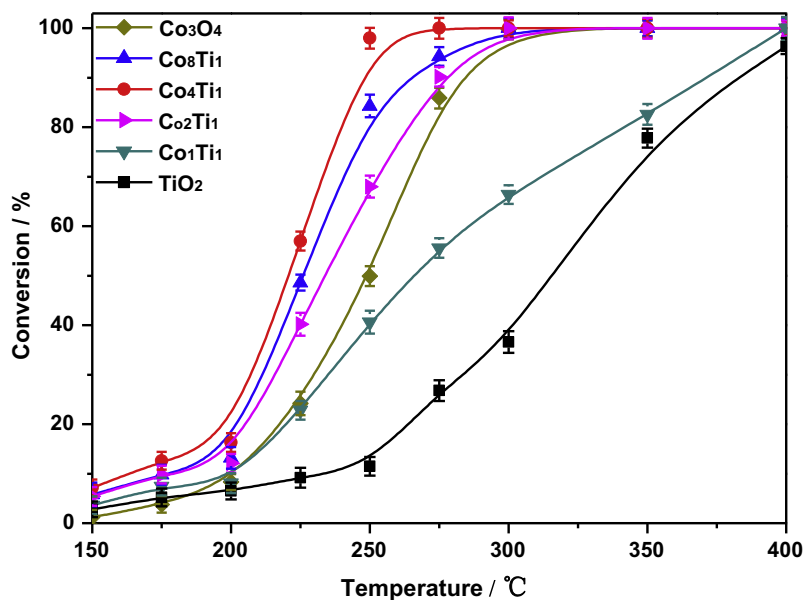
Fig. 9. CH_2Br_2 conversion over Ti-modified Co_3O_4 catalysts with various Co/Ti ratios; gas composition: 500 ppm CH_2Br_2, 10% O_2 and N_2 as the balance; GHSV = 60,000 h^{-1}.

confirmed that Co-O-Ti solid solutions were formed. Moreover, Co_1Ti_1 showed a weak band because of the significant distortion of the spinel structure. Pure TiO_2 showed three expected bands that were related to vibration modes of anatase TiO_2 (B_{1g} mode at 395 cm^{-1}, A_{1g} mode at 515 cm^{-1} and E_g mode at 639 cm^{-1}) [23]. The results were consistent with the XRD analysis, and they indicated there was a strong interaction between Co and Ti in the mixed oxide catalysts.

To obtain the microscopic morphology and structural information of the catalyst, TEM and HRTEM were conducted, and the corresponding images are presented in Fig. 5. Pure Co_3O_4 exhibited hexagonal prism with size varying from 25 to 40 nm. With the incorporation of Ti, nano-particles showed amorphous shape with size varying from 10 to 30 nm. HRTEM image of Co_4Ti_1 displayed two types of lattice fringed directions with interplanar spacing of 0.280 and 0.467 nm, corresponding to (2 2 0) and (1 1 1) planes of Co_3O_4 spinel [24]. The lattice fringe of crystal phase ascribed to Ti species was not observed, confirming that Ti species of Co_4Ti_1 entered Co_3O_4 spinel lattice to form $Ti_xCo_{3-x}O_4$ solid solution.

To investigate the surface element composition and element oxidation states of the catalyst, XPS was conducted, and the results are presented in Fig. 6 and listed in Table 2. As shown in Fig. 6(a), two main peaks, with satellite peaks, corresponding to Co $2p_{3/2}$ and Co $2p_{1/2}$ at 775–783 eV and 791–800 eV were observed, respectively. The main Co $2p_{3/2}$ spectra could be divided into two components. The peak at 778.7–780.0 eV was attributed to Co^{3+}, while the one at 779.8–781.5 eV was related to Co^{2+} [25]. As shown in Table 2, the relative ratio of Co^{3+}/Co^{2+} that was calculated using the curve-fitted data decreased in the order of $Co_4Ti_1 > Co_2Ti_1 > Co_8Ti_1 > Co_3O_4 > Co_1Ti_1$, indicating that some Co ions transitioned from Co^{2+} to Co^{3+} as the Ti species entered the spinel structure and most Ti species substituted for Co^{2+} in the tetrahedral sites. However, the decrease in Co^{3+}/Co^{2+} for Co_2Ti_1 and Co_1Ti_1 was due to the presence of Co_2TiO_4 where Co species mainly existed in the form of Co^{2+}. In Fig. 6(b), it can be seen that the binding energy of Ti $2p_{3/2}$ decreased from 459.5 eV for TiO_2 to 457.4 eV for Co_8Ti_1, indicating the reduction in the partial Ti^{4+} to low valence Ti in Ti-modified Co_3O_4 catalysts [26].

The O 1s spectra of Ti-modified Co_3O_4 catalysts are presented in Fig. 6(c), and the curves of O 1s spectra were divided into two components. The one with a binding energy of 528.9–529.7 eV was ascribed to the lattice oxygen (O_{lat}), while the other with a binding energy of 530.3–531.3 eV was assigned to the surface adsorbed oxygen (O_{ads}) [27]. For Co_3O_4, the binding energy of O_{lat} was 529.0 eV; with the incorporation of Ti, the binding energy of O_{lat} increased due to the "O→Ti" electron transfer process through the formation of Co-O-Ti solid solution. In other words, the mixed oxides were not physical mixtures of two different oxides; instead, they were a solid solution with the interaction of Co and Ti species. Hence, the behavior of O_{lat} species could be affected by Co-O-Ti solid solution. In addition, the ratio of O_{ads}/O_{lat} decreased with the incorporation of Ti, indicating that the contribution to O_{ads} was mainly from Co_3O_4. It is well known that Co_3O_4 had a considerable amount of active surface oxygen. The shift in the O_{ads} binding energy further suggested the interaction of Co and Ti species. Moreover, the ratio of O_{ads}/O_{lat}, which was calculated using the curve-fitted areas, decreased in the order of $Co_3O_4 > Co_4Ti_1 > Co_8Ti_1 > Co_2Ti_1 > Co_1Ti_1 > TiO_2$.

The reducibility of the catalyst was evaluated using H_2-TPR, and the results are presented in Fig. 7. For pure Co_3O_4, two reduction peaks at 337 and 387 °C were observed, which were ascribed to the reduction of Co^{3+} to Co^{2+} and Co^{2+} to Co^0, respectively [28]. After the incorporation of Ti, the first reduction peak shifted to a high temperature with a decrease in the peak area, which could be related to the substitution of Ti^{4+} for Co^{3+} in the octahedral sites. In addition, the formation of Co-O-Ti solid solution in the Co_3O_4 spinal structure could decrease the oxidation ability, which indicated that the oxidation ability of the Co^{3+} on Co_3O_4 was stronger than that of Ti-modified Co_3O_4 catalysts. However, no reduction peak was observed for pure TiO_2, indicating that it was difficult to reduce TiO_2.

It is well known that the surface acidic properties of the catalysts have a significant influence on the adsorption and oxidation of VOCs, which could be evaluated using NH_3-TPD. The NH_3-TPD profiles of Ti-modified Co_3O_4 catalysts are presented in Fig. 8. For pure Co_3O_4, two desorption peaks in the range of 50–300 and
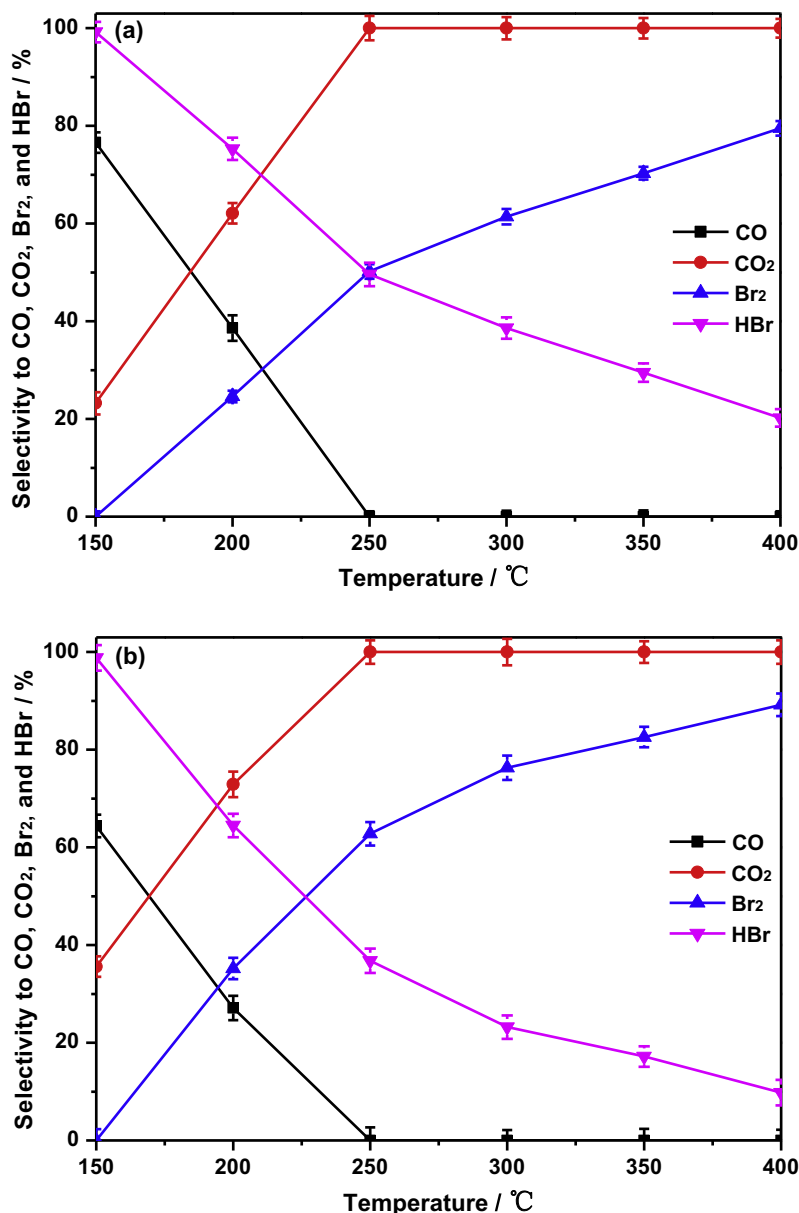
Fig. 10. The selectivity to CO, CO_2, Br_2, and HBr as a function of temperature over Co_3O_4 (a) and Co_4Ti_1 (b).

300–500 °C were observed, which were attributed to the weak and strong acid sites. With the incorporation of Ti, a broad peak in the range of 50–300 °C and a sharp desorption peak in the range of 300–500 °C were observed, and the areas of the peaks were larger than those of Co_3O_4. Moreover, the area of the peak gradually increased when the ratio of Co/Ti was 4 or higher, and the area of the peak gradually decreased when the ratio of Co/Ti was 2 or lower. The results indicated that the incorporation of suitable Ti could promote the formation of acid sites, especially strong acid sites. However, pure TiO_2 possessed fewer acid sites. In summary, the Ti-modified Co_3O_4 catalysts with more acid sites favor the adsorption and oxidation of CH_2Br_2.

3.2. Catalytic activity

The conversion curves of CH_2Br_2 oxidation over Ti-modified Co_3O_4 catalysts are presented in Fig. 9. Co_3O_4 had considerable activity with a T_{90} of approximately 287 °C. With the incorporation of Ti, the catalytic activity was significantly improved and the

conversion curves shifted to lower temperature, indicating that the formation of spinel $Ti_xCo_{3-x}O_4$ was conductive to CH_2Br_2 oxidation. Co_4Ti_1 exhibited the optimal catalytic activity with a T_{90} of approximately 245 °C. However, with the increase in Ti content up to Ti/Co = 1/2 or higher, the conversion curves shifted to a higher temperature and catalytic activity decreased. For instance, the T_{90} value for Co_1Ti_1 was approximately 372 °C. The catalytic activity of TiO_2 was the lowest, and the T_{90} value was only 386 °C, indicating that pure TiO_2 was not beneficial for CH_2Br_2 oxidation. Based on the T_{90} values, the sequence of the catalytic activity for CH_2Br_2 oxidation was as follows: $Co_4Ti_1 > Co_8Ti_1 > Co_2Ti_1 > Co_3O_4 > Co_1Ti_1 > TiO_2$.

3.3. Product selectivity

The analysis of products showed that the CH_2Br_2 decomposition products were mainly COx, H_2O, Br_2, and HBr, and no other Br-containing organic byproducts were formed (Table S1 and S2). However, the product selectivity was different and depended on
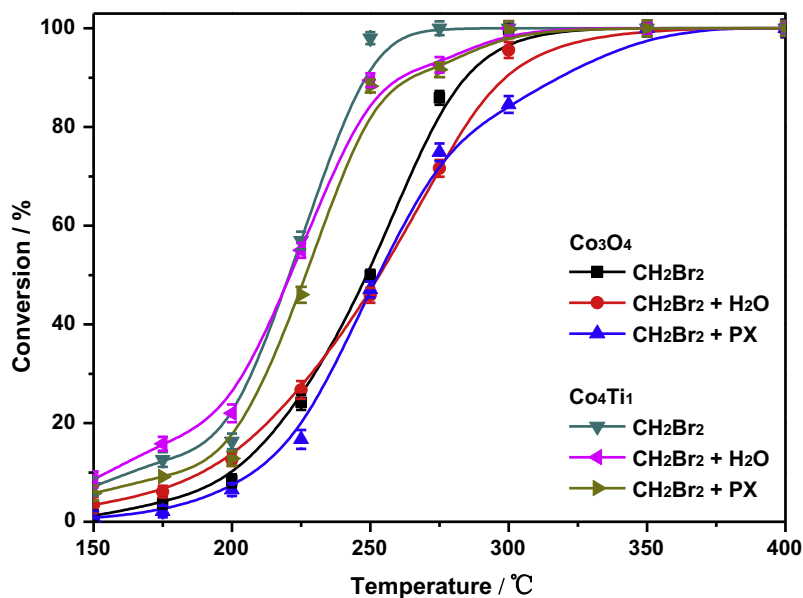
Fig. 11. The effect of water or p-xylene (PX) on CH_2Br_2 oxidation over Co_3O_4 and Co_4Ti_1; CH_2Br_2 alone: 500 ppm CH_2Br_2; $CH_2Br_2 + H_2O$: 500 ppm CH_2Br_2 + 2 vol% H_2O; $CH_2Br_2 + PX$: 500 ppm CH_2Br_2 + 500 ppm PX; in all cases, 10% O_2, and N_2 as the balance; and GHSV = 60,000 h^{-1}.
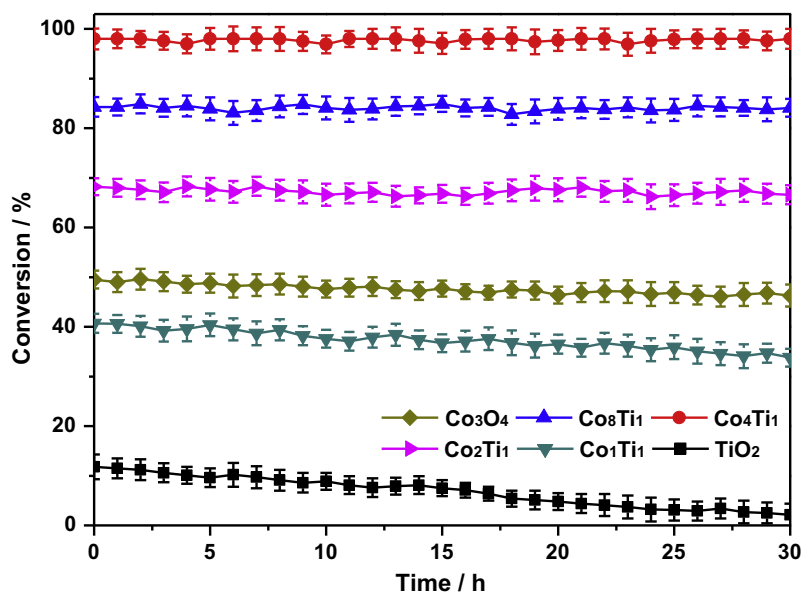
Fig. 12. Durability of Ti-modified Co_3O_4 catalysts with various Co/Ti ratios for CH_2Br_2 oxidation at 250 °C.

the catalyst. Fig. 10 shows the selectivity to CO, CO_2, Br_2, and HBr as a function of temperature over Co_3O_4 (a) and Co_4Ti_1 (b). For Co_3O_4, the selectivity to CO and HBr gradually decreased with increasing temperature, while the selectivity to CO_2 and Br_2 gradually increased. Similar results were also observed for Co_4Ti_1. The increase in the selectivity to CO_2 was attributed to the further oxidation of CO, and the selectivity levels to CO_2 were 23% and 62% at 150 and 200 °C, respectively, and which increased to 100% above 250 °C. In addition, Br_2 was generated when the temperature was higher than 200 °C, which might be due to the Deacon reaction ($4HBr + O_2 = 2Br_2 + H_2O$), and the selectivity to Br_2 reached 80% at 400 °C. For Co_4Ti_1, the selectivities to CO_2 were 36% and 73% at 150 and 200 °C, respectively, which was higher than that of

Co_3O_4. Moreover, the selectivity to Br_2 was higher than that of Co_3O_4 at each investigated temperature, and the selectivity to Br_2 reached 90% at 400 °C. The results indicated that the incorporation of Ti into Co_3O_4 contributed to the further oxidation of CO to CO_2 at a low temperature and promoted the generation of Br_2.

3.4. The effect of water and p-xylene (PX)

BVOCs-containing industrial exhaust gas usually contains water vapor, making it necessary to consider the water resistance ability of the catalyst. Hence, the CH_2Br_2 oxidation experiment was conducted in the presence of 2 vol% H_2O. As shown in Fig. 11, the CH_2Br_2 conversion over Co_3O_4 and Co_4Ti_1 decreased compared
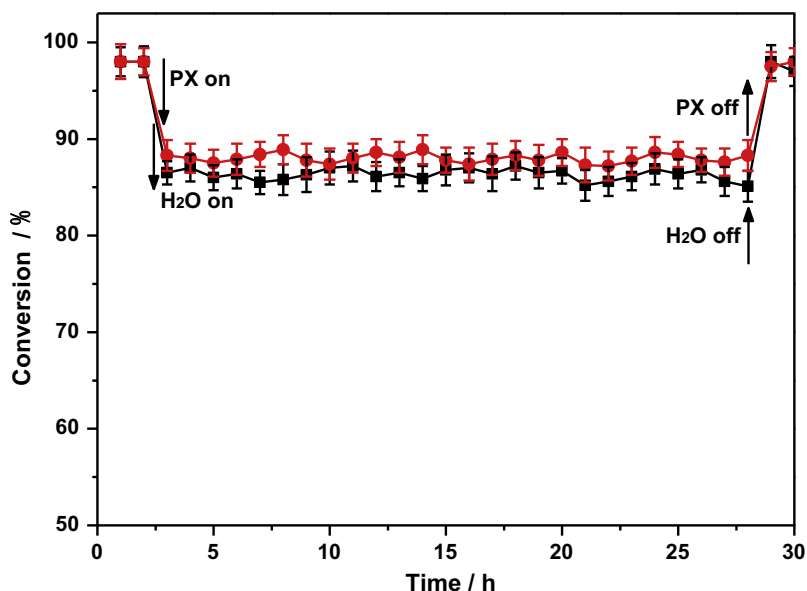
Fig. 13. Durability of Co_4Ti_1 in the presence of 2 vol% H_2O or 500 ppm PX for CH_2Br_2 oxidation at 250 °C.

with the results without H_2O at high temperature, and T_{90} increased by 14–16 °C because of the competitive adsorption between H_2O and CH_2Br_2 on active sites. However, an increased in CH_2Br_2 conversion was observed at low temperature, and T_{10} (the temperature needed for 10% conversion) decreased by 8–11 °C. The facilitating effect of H_2O on CH_2Br_2 oxidation at low temperatures might be related to the removal of surface bromine species based on the reverse Deacon reaction: $H_2O + Br^- \leftrightarrows HBr\uparrow + OH^-$ [29].

It is well known that BVOCs-containing industrial exhaust gas exhaust gas contains various organic compounds. However, it is unrealistic to simultaneously investigate the effect of various organic compounds on CH_2Br_2 oxidation. Therefore, we mainly studied the reaction characteristics involving binary organic pollutants; also, the effect of PX as a model PTA-exhaust-gas organic compound on CH_2Br_2 oxidation over Co_3O_4 and Co_4Ti_1 was studied. As shown in Fig. 11, in the presence of PX, the T_{90} values with Co_4-Ti_1 and Co_3O_4 were 261 and 322 °C, respectively, which increased somewhat compared with the results without PX (245 and 287 °C). The inhibition might be related to the decrease in the oxygen species caused by the consumption of surface-active oxygen in PX oxidation.

3.5. Catalyst durability

For practical application, it is significant to investigate the durability of Ti-modified Co_3O_4 catalysts. Fig. 12 presents the durability of Ti-modified Co_3O_4 catalysts for CH_2Br_2 oxidation at 250 °C. Within 30 h, Co_3O_4, Co_8Ti_1, Co_4Ti_1, and Co_2Ti_1 demonstrated highly stable activity. During the durability test, the product selectivity was nearly constant, showing that the composition and structure of the active component were stable. It is generally accepted that the accumulation of Br species on the Co_3O_4-based catalyst is the main cause of deactivation. XPS analysis indicated that the deposition levels of Br on the surface of Co_3O_4 and Co_4Ti_1 were 1.07% and 0.89% after 30 h of reaction, respectively, which showed that Co-O-Ti solid solution could promote the removal of Br species on the surface of Co_3O_4. However, the Co_1Ti_1 and TiO_2 activity levels gradually decreased, and the conversion of Co_1Ti_1 and TiO_2 decreased by 7% and 10%, respectively, indicating that Ti-modified Co_3O_4

catalysts with high Ti content were easily deactivated as Br species were deposited on Ti species.

It is necessary to investigate the durability of Co_4Ti_1 in the presence of 2 vol% H_2O or 500 ppm PX for CH_2Br_2 oxidation at 250 °C. As shown in Fig. 13, the CH_2Br_2 conversion was stable in approximately 98% of the samples within the first 2 h. After, 2 vol% H_2O was introduced into the reaction system, the CH_2Br_2 conversion decreased from 98 % to 86% and then remained constant for 26 h, indicating that H_2O had an inhibitory effect on CH_2Br_2 oxidation by occupying the active sites of the catalyst. When H_2O was removed, the CH_2Br_2 conversion could recover to 98%. This phenomenon indicated that CH_2Br_2 and H_2O had a competitive adsorption relationship on the catalyst surface. Moreover, a similar phenomenon was observed when 500 ppm PX was introduced into the reaction system. The results demonstrated that, in the presence of H_2O or PX, Co_4Ti_1 exhibited excellent durability for CH_2Br_2 oxidation in the long term reaction, making it promising for practical application.

3.6. In situ DRIFTs study

To explore deeply the intermediate species formed during the CH_2Br_2 catalytic oxidation, *in situ* DRIFTs experiments were conducted on Co_3O_4 and Co_4Ti_1, and the related spectra are shown in Fig. 14(a, b). As shown in Fig. 14(a), for Co_3O_4, after exposed to a gas stream of 500 ppm CH_2Br_2, 10% O_2, and N_2 balance at 50 °C for 1 h, bands at 3078, 2998, 1620, and 1200 cm^{-1} were observed. Bands at 3078, 2998, and 1200 cm^{-1} could be assigned to methylene species ($-CH_2-$) asymmetric stretching, symmetric stretching, and wagging, respectively, which approximately modeled CH_2Br_2 molecules adsorbed on the Co_3O_4 surface [30]. When the temperature was raised, the bands assigned to CH_2Br_2 molecules decreased in intensity and could not be observed above 100 °C, indicating either desorption or reaction of CH_2Br_2 molecules. The band at 1620 cm^{-1} was assigned to H_2O on the surface [31], which could gradually disappear as the temperature increased. Additionally, disappearance of the bands assigned to CH_2Br_2 molecules occurred with the appearance of some new bands at 1541, 1433, and 1348 cm^{-1}, which were assigned to asymmetric vibration, δ (CH_2), and symmetric vibration of adsorbed formate species
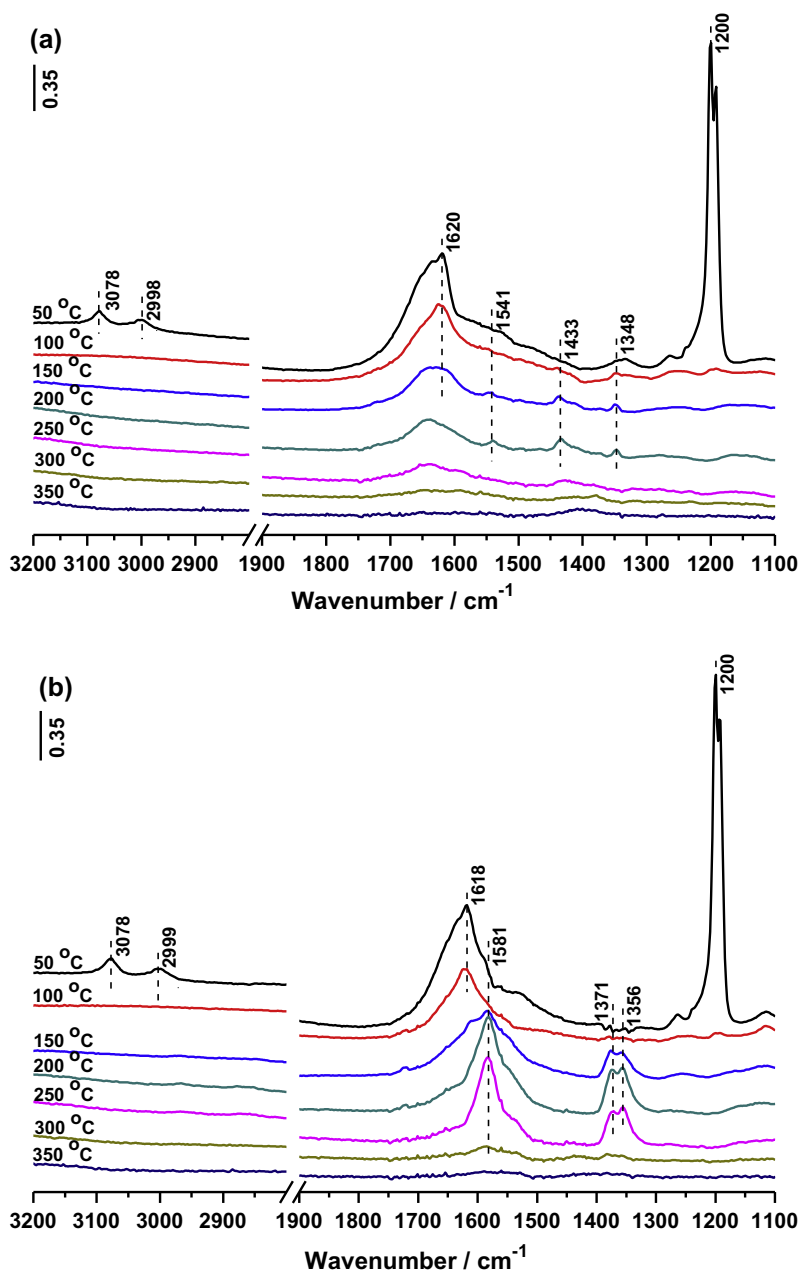
Fig. 14. *In situ* DRIFTs spectra of CH_2Br_2 oxidation over Co_3O_4 (a) and Co_4Ti_1 (b) at different temperatures.

(−COOH) [31]. When the temperature increased to 350 °C, no bands could be observed, indicating CH_2Br_2 had been completely oxidized. All bands formed in the process of CH_2Br_2 oxidation, implying that the formate species were the main intermediate products on the Co_3O_4 surface.

For Co_4Ti_1 (Fig. 14(b)), it was not surprising that the intensities of the bands assigned to CH_2Br_2 molecules were slightly higher than those for Co_3O_4 at 50 °C because of the stronger surface acidity. When the temperature increased, new bands at 1581, 1371, and 1356 cm^{-1} were observed, which were ascribed to the COO and CH stretching of adsorbed formate species (−COOH) [32,33]. The results implied that the formate species were the main intermediate products that formed on the surface of Co_4Ti_1, and the reaction pathway was not essentially changed with the incorporation of Ti. Additionally, no bands related to CO, CO_2, or HBr as the

final products were observed because of the quick desorption of these species.

To deeply understand this reaction, a receivable reaction mechanism for CH_2Br_2 oxidation over Ti-modified Co_3O_4 catalysts was proposed as follows (Fig. 15): (1) the adsorption of CH_2Br_2 on the active Co species (Co_3O_4, $CoTiO_3$, and Co_2TiO_4) as acid sites through bromine atoms; (2) the adsorbed CH_2Br_2 dissociated with the fracture of C-Br bonds into some intermediate products, such as formate species; (3) the adsorption of gas-phase oxygen on the catalyst surface supplemented the consumed oxygen; (4) the intermediate products were further oxidized by active oxygen species into CO and CO_2; (5) the promotion of removal of Br species by active oxygen species; and (6) the desorption of adsorbed Br species from the catalyst surface in the form of HBr and Br_2.
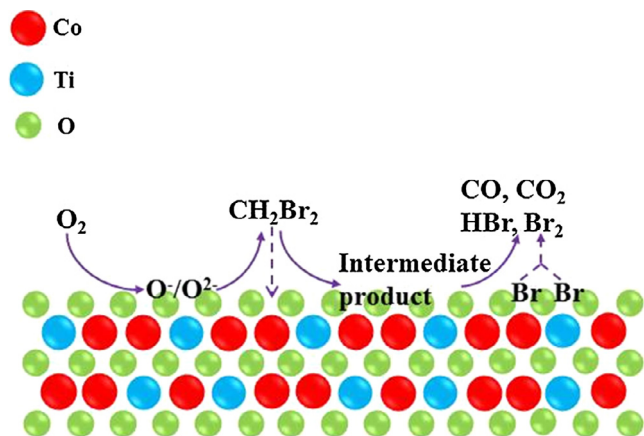
Fig. 15. A receivable reaction mechanism for CH_2Br_2 oxidation over Ti-modified Co_3O_4 catalysts.

4. Conclusions

In this study, a series of Ti-modified Co_3O_4 catalysts with various Co/Ti ratios was synthesized using the co-precipitation method and then were used in catalytic oxidation of CH_2Br_2, which was selected as the model molecule for BVOCs. Among all Ti-modified Co_3O_4 catalysts, Co_4Ti_1 achieved higher catalytic activity with a T_{90} of approximately 245 °C for CH_2Br_2 oxidation and higher selectivity to CO_2 at low temperature than the other investigated catalysts. XRD and Raman results showed that the incorporation of Ti into the Co_3O_4 spinel structure could distort the crystal structure. The surface acidity of the catalyst could be promoted by Ti. The high catalytic activity of Co_4Ti_1 was attributed to the high Co^{3+}/Co^{2+} ratio and high surface acidity. In addition, the synergistic effect of Co and Ti made it superior for CH_2Br_2 oxidation. The results of the long-duration stability experiments demonstrated that Co_4Ti_1 could be an excellent catalyst for CH_2Br_2 oxidation. Hence, the incorporation of Ti into Co_3O_4 catalysts could further improve the catalytic activity, stability, and product-selectivity of the Co_3O_4-based catalysts for CH_2Br_2 oxidation. Furthermore, based on the analysis of products and *in situ* DRIFTs studies, a receivable reaction mechanism for CH_2Br_2 oxidation over Ti-modified Co_3O_4 catalysts was proposed. However, the issue of deep oxidation (the oxidation of CO to CO_2) at low temperature still remained to be resolved.

Acknowledgements

Appendix A. Supplementary material

Supplementary data associated with this article can be found, in the online version, at http://dx.doi.org/10.1016/j.jcis.2017.06.077.

References

[1] T. Yue, X. Yue, F. Chai, J. Hu, Y. Lai, L. He, R. Zhu, Characteristics of volatile organic compounds (VOCs) from the evaporative emissions of modern passenger cars, Atmosp. Environ. 151 (2016) 62–69.

[2] A.R. Evanoski-Cole, K.A. Gebhart, B.C. Sive, Y. Zhou, S.L. Capps, D.E. Day, A.J. Prenni, M.I. Schurman, A.P. Sullivan, Y. Li, Composition and sources of winter haze in the Bakken oil and gas extraction region, Atmosp. Environ. 156 (2017) 77–87.

[3] J. Gao, A. Woodward, S. Vardoulakis, S. Kovats, P. Wilkinson, L. Li, X. Lei, L. Jing, J. Yang, L. Jing, Haze, public health and mitigation measures in China: a review of the current evidence for further policy response, Sci. Total Environ. 578 (2016) 148–157.

[4] M.S. Kamal, S.A. Razzak, M.M. Hossain, Catalytic oxidation of volatile organic compounds (VOCs) – A review, Atmosp. Environ. 140 (2016) 117–134.

[5] X. Huang, Catalytic combustion of PTA off-gas over Ce-Mn composite oxides, Environmental Engineering 29 (5) (2011) 97–98.

[6] J. Mei, Y. Ke, Z. Yu, X. Hu, Z. Qu, N. Yan, Morphology-dependent properties of Co_3O_4/CeO_2 catalysts for low temperature dibromomethane (CH_2Br_2) oxidation, Chem. Eng. J. 320 (2017) 124–134.

[7] X. Liu, J. Zeng, J. Wang, W. Shi, T. Zhu, Catalytic oxidation of methyl bromide using ruthenium-based catalysts, Catalys. Sci. Tech. 6 (12) (2016) 4337–4344.

[8] J. Mei, S. Zhao, H. Xu, Z. Qu, N. Yan, The performance and mechanism for the catalytic oxidation of dibromomethane (CH_2Br_2) over Co_3O_4/TiO_2 catalysts, RSC Adv. 6 (37) (2016) 31181–31190.

[9] W. Ahmad, T. Noor, M. Zeeshan, Effect of synthesis route on catalytic properties and performance of Co_3O_4/TiO_2 for carbon monoxide and hydrocarbon oxidation under real engine operating conditions, Catal. Commun. 89 (2016) 19–24.

[10] M. Jian, S. Zhao, W. Huang, Q. Zan, N. Yan, Mn-Promoted Co_3O_4/TiO_2 as an efficient catalyst for catalytic oxidation of dibromomethane (CH_2Br_2), J. Hazard. Mater. 318 (2016) 1–8.

[11] T. Cai, H. Hao, D. Wei, Q. Dai, L. Wei, X. Wang, Catalytic combustion of 1,2-dichlorobenzene at low temperature over Mn-modified Co_3O_4 catalysts, Appl. Catal. B: Environ. 166–167 (2015) 393–405.

[12] Z. Shi, P. Yang, F. Tao, R. Zhou, New insight into the structure of CeO_2-TiO_2 mixed oxides and their excellent catalytic performances for 1,2-dichloroethane oxidation, Chem. Eng. J. 295 (2016) 99–108.

[13] D. Vernardou, E. Stratakis, G. Kenanakis, H.M. Yates, S. Couris, M.E. Pemble, E. Koudoumas, N. Katsarakis, One pot direct hydrothermal growth of photoactive TiO_2 films on glass, J. Photochem. Photobiol. A Chem. 202 (2–3) (2009) 81–85.

[14] G. Kenanakis, D. Vernardou, A. Dalamagkas, N. Katsarakis, Photocatalytic and electrooxidation properties of TiO_2 thin films deposited by sol-gel, Catalysis Today 240 (3) (2015) 146–152.

[15] D. Vernardou, K. Vlachou, E. Spanakis, E. Stratakis, N. Katsarakis, E. Kymakis, E. Koudoumas, Influence of solution chemistry on the properties of hydrothermally grown TiO_2 for advanced applications, Cataly. Today 144 (1–2) (2009) 172–176.

[16] Y.Y. Can, Cao, Hui Zhang, Jian Xie, Shichao Zhang, Bin Pan, Gaoshao Cao, Xinbing Zhao, Controlled Growth of Li_2O_2 by Cocatalysis of Mobile Pd and Co_3O_4 Nanowire Arrays for High-Performance Li-O_2 Batteries, ACS Appl. Mater. Interf. 8 (2016) 31653–31660.

[17] T. Acharya, R.N.P. Choudhary, Structural, dielectric and impedance characteristics of $CoTiO_3$, Mater. Chem. Phys. 177 (2016) 131–139.

[18] S. Zhang, M. Ye, A. Han, C. Liu, Preparation and characterization of Co_2TiO_4 and doped $Co_{2−x}M_xTiO_4$ ($M = Zn^{2+}$, Ni^{2+})-coated mica composite pigments, Appl. Phys. A 122 (7) (2016) 1–9.

[19] Y.F. Zhao, C. Li, S. Lu, L.J. Yan, Y.Y. Gong, L.Y. Niu, X.J. Liu, Effects of oxygen vacancy on 3d transition-metal doped anatase TiO_2: First principles calculations, Chem. Phys. Lett. 647 (2016) 36–41.

[20] L. Chen, F. Hu, H. Duan, Q. Liu, H. Tan, W. Yan, T. Yao, Y. Jiang, Z. Sun, S. Wei, Intrinsic ferromagnetic coupling in Co_3O_4 quantum dots activatedby graphene hybridization, Appl. Phys. Lett. 108 (25) (2016) 1929.

[21] S. Yuvaraj, R.H. Vignesh, L. Vasylechko, Y.S. Lee, R.K. Selvan, Synthesis and electrochemical performance of Co_2TiO_4 and its core-shell structure of Co_2TiO_4@C as negative electrodes for Li-ion batteries, RSC Adv. 6 (73) (2016) 69016–69026.

[22] Y.K. Sharma, M. Kharkwal, S. Uma, R. Nagarajan, Synthesis and characterization of titanates of the formula $MTiO3$ (M=Mn, Fe Co, Ni and Cd) by co-precipitation of mixed metal oxalates, Polyhedron 28 (3) (2009) 579–585.

[23] B.P. Laskova, L. Kavan, M. Zukalova, K. Mocek, O. Frank, In situ Raman spectroelectrochemistry as a useful tool for detection of TiO_2 (anatase) impurities in TiO_2 (B) and TiO_2 (rutile), Monatshefte für Chemie-Chem. Monthly 147 (5) (2016) 951–959.

[24] X. Xie, Y. Li, Z.Q. Liu, M. Haruta, W. Shen, Low-temperature oxidation of CO catalysed by Co_3O_4 nanorods, Nature 458 (7239) (2009) 746–749.

[25] W. Chao, H. Ying, M. Chen, Y. Jing, Y. Wen, X. Chen, Fabrication of porous nanosheets assembled from $NiCo_2O_4/NiO$ electrode for electrochemical energy storage application, J. Colloid Interf. Sci. 504 (2017) 1–11.

[26] W. Deng, Q. Dai, Y. Lao, B. Shi, X. Wang, Low temperature catalytic combustion of 1,2-dichlorobenzene over CeO_2-TiO_2 mixed oxide catalysts, Appl. Catal. B: Environ. 181 (2016) 848–861.

[27] T. Zp, S. K, C. FR, N. OM, M. GH, M. DE, Ultra-sensitive and selective NH_3 room temperature gas sensing induced by manganese-doped titanium dioxide nanoparticles, J. Colloid Interf. Sci. 504 (2017) 371–386.

[28] T. Nyathi, N. Fischer, A. York, M. Claeys, Effect of crystallite size on the performance and phase transformation of Co_3O_4/Al_2O_3 catalysts during CO-PrOx - An in situ study, Faraday Discuss. 197 (2017) 269–285.

[29] C.E. Hetrick, F. Patcas, M.D. Amiridis, Effect of water on the oxidation of dichlorobenzene over V_2O_5/TiO_2 catalysts, Appl. Catal. B: Environ. 101 (3–4) (2011) 622–628.

[30] M.T. Chen, C.F. Lien, A. Lifen Liao, J.L. Lin, In-Situ FTIR Study of Adsorption and Photoreactions of CH_2Cl_2 on Powdered TiO_2, J. Phys. Chem. B 107 (16) (2003) 3837–3843.

[31] W. Yu, A.P. Jia, M.F. Luo, J.Q. Lu, Highly active spinel type $CoCr_2O_4$ catalysts for dichloromethane oxidation, Appl. Catal. B: Environ. 165 (2015) 477–486.

[32] J. Su, W. Yao, Y. Liu, Z. Wu, The impact of CrOx loading on reaction behaviors of dichloromethane (DCM) catalytic combustion over Cr-O/HZSM-5 catalysts, Appl. Surf. Sci. 396 (2016) 1026–1033.

[33] S. Cao, H. Wang, F. Yu, M. Shi, S. Chen, X. Weng, Y. Liu, Z. Wu, Catalyst performance and mechanism of catalytic combustion of dichloromethane (CH_2Cl_2) over Ce doped TiO_2, J. Colloid Interf. Sci. 463 (2015) 233–241.